

## Mechanics Of Interfacial Crack Propagation In Microscratching

San Franc.

Maarten P. de Boer\*, John C. Nelson and William W. Gerberich

Dept. of Chemical Engineering and Materials Science, University of Minnesota, Minneapolis, MN 55455. \*Present address - Sandia National Laboratories, Albuquerque, NM 87185 MS 1413

4/8/96

**Abstract**

A new probing technique has been developed to test thin film mechanical properties. In the Microwedge Scratch Test (MWST), a wedge shaped diamond indenter tip is drawn along a fine line, while simultaneously being driven into the line. We compare microwedge scratching of Zone 1 and Zone T thin film specimens of sputtered W on  $\text{SiO}_2$ . Symptomatic of its poor mechanical properties, the Zone 1 film displays three separate crack systems. Because of its superior grain boundary strength, the Zone T film displayed only one of these - an interfacial crack system. Using bimaterial linear elastic fracture mechanics, governing equations are developed for propagating interfacial cracks, including expressions for strain energy release rate, bending strain, and mode mixity. Grain boundary fracture strength information may be deduced from the Zone 1 films, while adhesion may be inferred from the Zone T films.

MAY 17 1996

**Introduction**

There are two main issues regarding thin film debonding. The first is the *nucleation* of interfacial cracks, while the second is the *propagation* of cracks. From a mechanical testing point of view, scratch testing [1-3] primarily serves to address the former issue, while indentation testing [4, 5] is a method of addressing the latter. To date, the results of the two tests cannot be quantitatively compared with good confidence. This is for two reasons. First, the scratch test geometry is three dimensional, while indentation test mechanics analysis is based on an axisymmetric geometry. Second, in the scratch test a critical load drop is measured which may be associated with a complicated elastic-plastic stress distribution near the indenter tip, while the indentation analysis applies to a crack tip significantly removed from the indenter tip so that linear elastic conditions apply. The objective of this work is to relate the work of adhesion,  $\Gamma_i$ , in the scratch test to  $\Gamma_i$  in the indentation test. This is done by considering *crack propagation* in the two cases. Both types of tests have been placed in a plane strain geometry to simplify the comparisons. The sample is a thin film fine line, rather than a planar thin film. The mechanical probe is a microwedge, rather than a conical tip. The associated mechanics and experimental results [6, 7] for the Microwedge Indentation Test (MWIT) have been reported. Here, we investigate the Microwedge Scratch Test (MWST), compare it to the MWIT, show how the mechanics are related and that similar values for adhesion arise.

The important variable in this study is that one film has a Zone 1 microstructure (voided grain boundaries), while the other has a Zone T microstructure (metallurgical grain boundaries) [8]. Sputtered W on  $\text{SiO}_2$  is used as the experimental system of interest, as it is common in the microelectronics industry, can exhibit poor adhesion especially when subject to high tensile stresses of chemical vapor deposition, and exhibits brittle failure so that bimaterial linear elastic fracture mechanics [9] is applicable.

**Experimental**

Silicon wafers were thermally oxidized to 1  $\mu\text{m}$  thickness. Zone 1 and Zone T films were obtained by rf-sputtering at 20 and 13 mtorr respectively. The residual stress of these films measured by wafer curvature was 15 and 100 MPa, small compared to stresses induced by the microwedge. Zone 1 grains were about 20 nm in diameter, while Zone T film grains were bimodal in size distribution, with large elongated grains, in agreement with ref. [10]. Photolithography and wet etching was employed to define long lines of 10  $\mu\text{m}$  width. A 20  $\mu\text{m}$  wide diamond 90° included angle microwedge with a flattened surface of 0.7  $\mu\text{m}$  was used for scratching. The microwedge was mounted to a continuous microindenter system [11] with normal load resolution of 16  $\mu\text{N}$  and depth resolution of 0.5 nm. A spring activated tangential load cell was

**MASTER**DISTRIBUTION OF THIS DOCUMENT IS UNLIMITED *1996*

## **DISCLAIMER**

**Portions of this document may be illegible  
in electronic image products. Images are  
produced from the best available original  
document.**

constructed, and its resolution is 50  $\mu\text{N}$ . Three of the four outputs (scratch distance  $SD$ , normal load  $P_{\text{norm}}$ , depth  $D$ , and tangential load  $P_{\text{tang}}$ ) could be monitored during any given test. The coefficient of friction  $cof = P_{\text{tang}}/P_{\text{norm}}$ . At the end of the scratch test, the wedge tip was removed vertically from the substrate. Results of the mechanical testing were observed ex-situ by SEM on a JEOL 840 instrument with a  $\text{LaB}_6$  filament.

In the first series of tests, the scratch speed was 0.5  $\mu\text{m/sec}$ . At moderate loads as denoted by region "A" in Fig. 1a, tensile cracking behind the indenter tip occurs due to voided grain boundaries characteristic of Zone 1 films. These lead to the "delamination crack" seen in Fig. 1b.

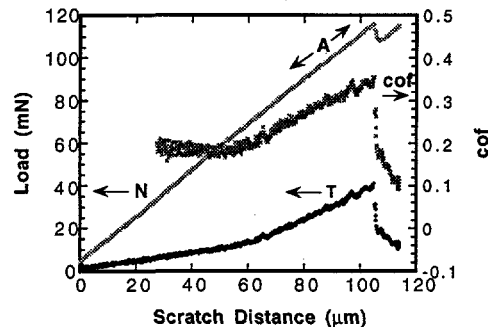


Fig. 1a  $P_{\text{norm}}$  and  $P_{\text{tang}}$  and  $cof$  vs.  $SD$

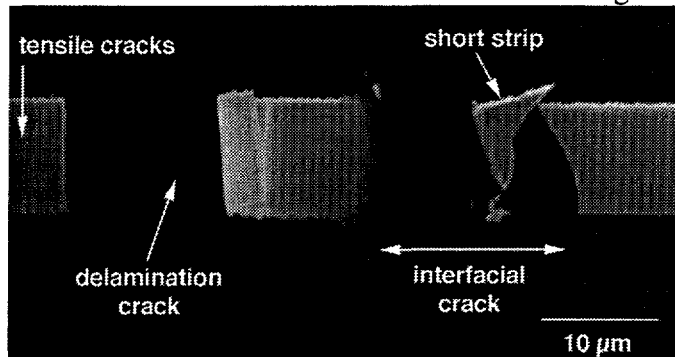


Fig. 1b Associated SEM fractograph

As  $P_{\text{norm}}$  increases above 60 mN in Fig. 1a, pileup of the tungsten thin film in front of the indenter tip causes the  $cof$  to rise, due to grooving in the film. At a critical load  $P_{\text{norm},c}$ , a load drop occurs. This is associated with an "interfacial crack" system in front of the indenter tip, as labeled in Fig. 1b. The final interfacial crack length is determined by a spallation event, as will be shown. A value of  $cof = 0.35$  at  $P_{\text{norm},c}$  will be used for the Zone 1 film. Also seen in Fig. 1b is a short strip in front of the microwedge which has been pushed ahead by a scratch distance approximately equal to the travel after the load drop. As the indenter tip continues its motion after the load drop, the short strip in front of it is broken off, and the tip strikes the substrate, where  $P_{\text{norm}}$  begins to rise again. This is called the "short strip" crack system. A magnified view of  $P_{\text{norm}}$  and  $P_{\text{tang}}$  vs.  $SD$  near  $P_{\text{norm},c}$  revealed a sudden load drop of  $P_{\text{norm}}$  and  $P_{\text{tang}}$  after  $P_{\text{norm},c}$ , suggesting a significant change in compliance of the sample.

In order to obtain greater insight into the sequence of events, an investigation of the  $P_{\text{norm}}$  curve near  $P_{\text{norm},c}$  was undertaken. The scratch speed was reduced to 0.1  $\mu\text{m/sec}$ , the minimum available on the system. Data collection rate was increased to 12 per channel per second. The wedge motion was stopped with 0.1  $\mu\text{m}$  accuracy at various points of interest on the  $P_{\text{norm}}$  vs.  $SD$  curve, as monitored on a strip chart. The depth reading from the strip chart gave the greatest in-situ signal with regard to critical events. SEM micrographs of samples from which the wedge was removed just before the load drop indicated no interfacial cracking. Had an interfacial crack initiated at this point, it would remain open due to induced residual stress. Just after the load drop, interfacial cracking and spallation had both already taken place. It was not possible to obtain a stable crack for the Zone 1 films.

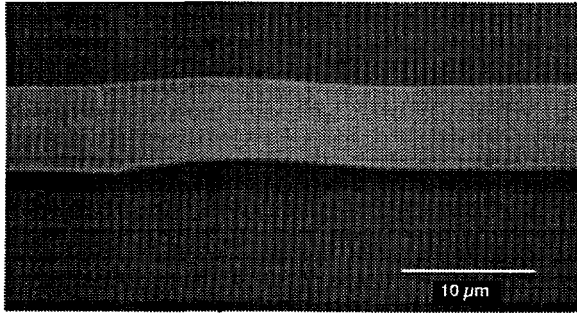


Fig. 2a  $SD=0.15 \mu\text{m}$  after  $P_{\text{norm},c}$  - buckle shape.

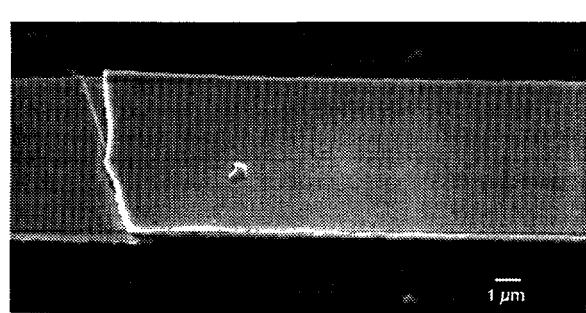


Fig. 2b  $SD=2.0 \mu\text{m}$  after  $P_{\text{norm},c}$  - film detaches

The  $0.5 \mu\text{m}$  thick Zone T film was tested next. As seen in Fig. 2a, a buckle shape leading to a stable crack of  $26 \mu\text{m}$  length now forms. Scratching was stopped about  $0.15 \mu\text{m}$  after  $P_{\text{norm},c}$  was reached for this sample.  $P_{\text{norm},c}$  is  $85 \text{ mN}$ , lower than for the Zone 1 film, in part because it is thinner. A close-up of the area near the indenter tip reveals an initiation of film fracture near the indenter tip. There is only minor tensile cracking behind the indenter tip, and no evidence of a delamination crack. This may be attributed to the greater Zone T grain boundary strength. For the Zone T films, there is no apparent "short strip" pushed out in front of the indenter tip.

A good correlation existed for length of the crack vs. scratch distance after the load drop. However, if scratching continued for too long, no crack at all was observed. Fig. 2b shows a line in which scratching continued for  $2 \mu\text{m}$  after the load drop. Rather than exhibiting an even longer interfacial crack, the line overlays the original line near the indenter tip. Apparently, after the indenter tip was removed, the line recoiled, and snapped over the bonded part of the line behind the indenter tip. Given that the line was originally in slight tension, it is surprising that the freed film has increased in length. It is believed that large residual compression has been induced into the line both behind and ahead of the indenter tip. When the tip is removed the compression relaxes, so that the freed film actually increases in length in its unstressed state. Likely, the crack length was much greater than  $50 \mu\text{m}$ , but once the driving force was removed, it lay back down, and the interfacial crack is imperceptible.

Although the Zone T film did not spall, a load drop, while smaller, was detectable. Hence, for the Zone T film the load drop can be associated with the large decrease in stiffness of a buckled film in comparison with an unbuckled film. As for the Zone 1 film, a larger change in  $P_{\text{tang}}$  than  $P_{\text{norm}}$  accompanied the load drop. For the Zone T films, a significantly smaller  $\text{cof} = 0.1$  was measured. It is believed that this is due to less plastic deformation, resulting in less plowing in front of the tip, and perhaps less adhesion between the indenter tip and the film.

### Expression for $G$

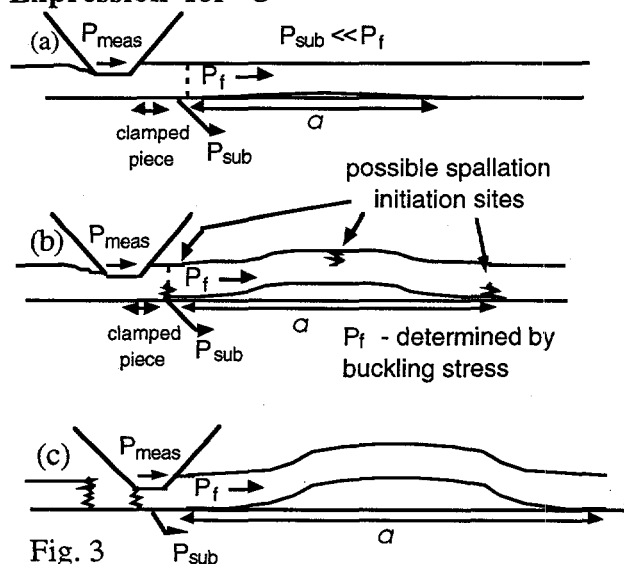


Fig. 3

An overall schematic of the sequence of events is constructed, as seen in Fig. 3. Once the interfacial crack nucleates, the tangential load is substantially higher than that required for propagation, and the crack rapidly extends as in Fig. 3a. Buckling ensues as in Fig. 3b. If the bending strains are survived, crack extension continues with further motion of the indenter tip (Fig. 3c). For the interfacial crack system, an approach well founded in fracture mechanics regarding adhesion and spallation is to find the strain energy release as a function of crack length,  $G \equiv \pm \partial U / \partial A$  at the advancing end of the crack front ( $U$  is the system strain energy, and  $A$  is the surface area created). A combination of the idealized thin film post-buckling theory and elastic half-space line loading of the substrate are used to find  $G$ .

While the crack propagates, the tangential

forces are not carried by the film alone. If  $P_f$  is the tangential load (per unit width) carried by the thin film, and  $P_s$  the tangential load (per unit width of the thin film) carried by the substrate,

$$P_f = \xi P_{\text{meas}}, \quad (1a)$$

$$\text{and} \quad P_s = [1 - \xi(a)] P_{\text{meas}} \quad (1b)$$

where  $\xi$  is a fraction between 0 and 1 best determined by detailed elastic-plastic considerations. In Fig. 3,  $P_{\text{meas}} = P_{\text{tang}} / b$  is the measured tangential load per unit width of the line.  $\xi$  is a weak function of crack length  $a$  before buckling because in the solution for tangential line loading of an elastic half space [12], shear stresses near the surface approach 0. The substrate strain energy must be considered because of the long range contribution from the elastic field of the tangential

contact transferred by friction to the substrate. Near the surface in the tangential direction stresses from  $P_{norm}$  are small [12]. Therefore the interfacial crack propagation driven by the linear elastic stress field outside the indenter tip plastic zone is dominated by  $P_{meas}$ . A fixed load condition is assumed in taking  $G = G_f + G_s$ . Given the weak dependence of  $\xi$  on  $a$ ,  $G_s \approx 0$ , before buckling it may be shown that

$$G \approx G_f = \frac{\xi^2(a)P_{meas}^2}{2hE_f}. \quad (2)$$

The buckling condition is satisfied when induced stress  $\sigma_e$  equals the Euler buckling stress  $\sigma_c$ :

$$\sigma_e = \frac{\xi P_{meas}}{h} = \sigma_c = \frac{\pi^2 E_f}{3} \left( \frac{h}{a_c} \right)^2, \quad (3a)$$

$$\text{or } a_c = \frac{\pi}{\sqrt{3}} h \left[ \frac{E_f}{(\xi P_{meas} / h)} \right]^{1/2}. \quad (3b)$$

where  $a_c$  is the critical crack length for buckling. After buckling, the load carried by the film is determined by the buckling stress, while  $P_s = P_{meas} - \sigma_c h$ , where  $P_s$  is the tangential load per unit width transferred to the substrate through the film which remains under the indenter tip. At the buckling condition where  $a = a_c$ ,  $P_f$  may be associated with an effective plastic displacement

$$P_f = (\Delta_{eff} / a_c) h E_f. \quad (4)$$

Equivalently, this may be associated with an effective plastic volume at the indenter tip

$$V_{eff} = \Delta_{eff} b h.$$

The source of buckling amplitude is lateral displacement of the film near the indenter tip. Because of the spring loading of the tangential load cell, the indenter tip surges forward as the tangential load drops, corresponding to a volume  $V_{ld}$ , or a displacement  $\Delta_{ld} = V_{ld} / bh$ . Crack extension continues resulting in one of two possible events. The first possibility is spallation due to large bending strains, as in Fig. 4b. The second possibility is crack arrest, which will occur if the initial surge in  $V_{ld}$  is survived. If crack stability is reached, continued forward displacement,  $\Delta_{for}$ , of the indenter tip creates further displacement, such that

$$\Delta_{elf} = \Delta_{eff} + \Delta_{ld} + \Delta_{for}. \quad (5)$$

A total volume  $V_{elf} = \Delta_{elf} b h$  is swept out by this process. As  $V_{elf}$  increases, crack extension continues. The standard expression  $G_f = \sigma^2 h / 2 E_f$  inherent in (2) must be modified to account for buckling. Furthermore, the substrate strain energy now changes with crack length, and can no longer be ignored. From a fixed grip analysis, the resulting expression is [13]

$$G = G_f + G_s = \frac{(\sigma_{elf})^2 h}{2E_f} \left[ 4 \left( \frac{\sigma_c}{\sigma_{elf}} \right) - 3 \left( \frac{\sigma_c}{\sigma_{elf}} \right)^2 \right] - \frac{(\sigma_e)^2 h}{E_s} \left( \frac{4 \eta h}{ba} \right) \left[ \left( \frac{\sigma_c}{\sigma_e} \right) - \left( \frac{\sigma_c}{\sigma_e} \right)^2 \right], \quad (6)$$

where  $\sigma_{elf} = E_f \Delta_{elf} / a$  is the stress that would be induced in the film were it not for buckling. The first term in (6) represents  $G_f$  accounting for buckling, while the second is due to the increasing substrate load as the crack extends, which reduces the effective stress intensity. Buckling and transfer of load to the substrate result in crack stability, but only if spallation does not occur first. The ultimate crack length depends on when the scratch test is stopped, because  $V_{elf}$  will increase  $V_{for}$  with as the scratch test proceeds.

An analytical form for the total strain  $\varepsilon_t$  vs.  $a$  can be determined from one-dimensional buckling theory by superimposing bending and compressive strains [13]. Likewise an analytical expression for the phase angle  $\Psi$  vs.  $a$  describing the mode mixity has been developed [13] using bimaterial linear elastic fracture mechanics [9].  $\Psi$  decreases from  $53^\circ$  before buckling continuously to  $-37^\circ$  after buckling as  $\Delta_{for}$  increases.

### Assessment of $G$ , $\varepsilon$ and $\Psi$

The measured data are given in Table 1. In this assessment of the model, it is assumed that  $\xi = 1$ . This is reasonable given that the film is much stiffer than the substrate (also  $P_{norm}$  will increase  $P_f$ ). The value for  $E_s$  is taken to be 150 GPa, since the substrate elastic strain energy is

dominated by silicon under the silica. As reported above, the *cof* was found to be 0.35 and 0.1 for the Zone 1 and Zone T films respectively. For the Zone 1 film,  $E_f=400$  GPa, while  $E_f=445$  GPa for the Zone T, with  $v_f = 0.28$ . The value for  $\Delta_{\text{eff}} = (\pi / \sqrt{3}) (P_{\text{meas}} h / E_f)^{1/2}$  is calculated consistent with (3a). In the assessment of  $\Delta_{\text{for}}$  for the Zone T films it is assumed that slippage between the indenter tip in the film is negligible after the load drop, and that the crack does not relax after the indenter tip is removed. For the Zone T data, the film remained attached near the indenter tip, so that crack relaxation should have been small.

**Table 1 - Measured data**

Zone	$h$ (μm)	$a$ (μm)	$b P_{\text{tang}}$ (mN)	$b$ (μm)	$\Delta_{\text{eff}}$ (μ)	$\Delta_{ld}$ (μm)	$\Delta_{\text{for}}$ (μm)
1	1.0	20	48.0	9.0	0.209	(0.067)	-
1	0.8	14	42.0	8.7	0.178	(0.083)	-
T	0.45	26	8.5	8.5	0.059	-	0.15
T	0.45	40	9.0	8.5	0.058	-	0.4
T	0.45	49	8.75	8.5	0.058	-	0.6

**Table 2 - Calculated Data**

Zone	$\Delta_c(a)$ (μ)	$a_c$ (μm)	$G_f$ (J/m <sup>2</sup> )	$G_s$ (J/m <sup>2</sup> )	$G$ (J/m <sup>2</sup> )	$\varepsilon$ (%)	$\Psi$ (°)
1	0.1645	15.7	47.2	-16.7	<b>30.5</b>	<b>0.75</b>	7
(1)	0.1645	15.7	74.1	-16.7	57.5	1.59	-6
1	0.1504	11.8	48.2	-18.0	<b>30.2</b>	<b>0.52</b>	12
(1)	0.1504	11.8	72.8	-18.0	54.9	2.12	-7
T	0.026	11.6	3.3	-0.7	<b>2.7</b>	<b>0.88</b>	-27
T	0.0167	11.4	2.4	-0.2	<b>2.2</b>	<b>0.78</b>	-32
T	0.0136	11.5	1.5	-0.1	<b>1.3</b>	<b>0.63</b>	-33

Tables 1 and 2

The  $\Delta_{ld}$  column in Table 1 was calculated for the Zone 1 films by assuming that the tangential load drop was 3 times the normal load drop, i.e. 2.4 mN (as calculated from the high data rate test.) Then  $\Delta_{ld}=2.4 \text{ mN} / k$ , where  $k=1.63 \times 10^4 \text{ N/m}$  is the tangential load cell spring constant. The data has been corrected for compression of the substrate as calculated from the tangential line loading solution in elasticity theory [14] (otherwise  $\Delta_{ld}$  would be still larger). For the Zone T films,  $\Delta_{ld}$  is neglected because it is small, and the small tension in the films approximately compensates it.

The values for  $G$ ,  $\varepsilon$  and  $\Psi$  are calculated at the measured  $a$ 's and reported in Table 2. For the spalled Zone 1 films,  $G$  is very high compared with the known  $\Gamma_i \approx 0.5 \text{ J/m}^2$  from the MWIT [7]. Therefore, the crack cannot yet be stable. Furthermore, values for  $\varepsilon$  and  $\Psi$  are close to those which accounted for spallation in the MWIT [7] ( $\varepsilon_{\text{max}}=0.4\%$  and  $\Psi=7^\circ$ ). Note the distinction made between calculations made for  $\Delta_{ld}=0$  and  $\Delta_{ld} \neq 0$ . If  $\Delta_{ld}$  is used, then the values for  $G$  and  $\varepsilon$  are even larger, and the above statements still hold. *This corroborates the experimental inference that spallation occurs before the next data point can be taken for the Zone 1 films.* For the Zone T films, the values for  $G$  are reasonably close to those measured more accurately [15] where  $\Gamma_i \approx 0.7 \text{ J/m}^2$  was found, as are the values of strain where a strain of 0.5 % was survived. Stable cracks grow according to (6), and they do not spall because the critical strain (fracture toughness) of the Zone T film is not exceeded. As expected by the strong dependency of  $\Psi$  on  $\Delta_{\text{for}}$ , the phase angle is near the minimum of  $-37^\circ$  for these films.

The phenomena are explained well by the theory presented. Better numerical accuracy can be achieved with more precise evaluation of  $\xi$  ( $\xi=1$  overestimates the true value, making the calculated values somewhat high), improved modeling of the buckling phenomena, and in-situ evaluation of  $\Delta_{\text{for}}$ . Also, the effect of  $P_{\text{norm}}$  on  $\xi$ , at present ignored, requires further consideration. A primary reason why the Zone 1 films spall is simply that the measured tangential force at spallation is greater. In effect, the Zone 1 is subject to a double jeopardy. First, nucleation of the crack is influenced primarily by the normal load, which is much larger in magnitude than the tangential load, and dominates shear at the interface near the indenter tip. The *cof* for the Zone 1

film is higher. Therefore, once it is nucleated, a much higher driving force induces larger bending strains. Second, the Zone 1 film has weaker grain boundaries.

A major drawback in the MWIT [7] was that substrate cracking rendered the calculated effective stresses invalid. In spite of the need to resort to effective displacements in the present model (inherently less accurate than load measurement for scratch testing), the results are quite good. This may be traced to the absence of substrate cracking in the MWST. As  $\Delta_{\text{for}}$  increases, the first term of (6) becomes the major contribution to  $G$ . Also, the effect of  $P_{\text{norm}}$  becomes minimal because the post-buckling behavior for eccentrically and perfectly aligned beams merges at large  $a$ . Therefore, although  $\xi=1$  is too high, the choice of its value becomes less important and the  $\Gamma_i=1.3 \text{ J/m}^2$  at  $a=49 \mu\text{m}$  (bottom row of Table 2) becomes quite close to the known value of  $\Gamma_i \approx 0.7 \text{ J/m}^2$ . It is believed that the above results are directly applicable to the conical tip scratch test of a planar film. Although then a 3-D stress problem must be solved, mixed mode I, II and III crack resistance in a basis 3 space can conceivably result.

### Summary and conclusions

In part due to the bluntness of the wedge (as required to survive scratching of the hard W film), there is some difficulty in nucleating an interfacial crack. Once it nucleates, the crack is overdriven, growing unstably until buckling. In the case of a Zone 1 film, the bending strains result in spallation. For the Zone T film, a stable interfacial crack is observed *if scratch motion is ended soon after the load drop*. The buckling and transfer of tangential load to the substrate act in concert to bring about a stable crack. Quantitative results from the model developed are in good agreement with this scenario. For stable cracks (Zone T films), the somewhat high values of  $\Gamma_i$  may be explained because in reality  $\xi < 1$ . The present article shows the relationship between the indentation and scratch testing for the case of plane strain.

### Acknowledgments

This work was supported by ONR under grant No. N00014-89-J-1726. M.P.dB. acknowledges the University of Minnesota Graduate School for a doctoral dissertation fellowship.

### References

1. P. Benjamin and C. Weaver, Proc. Roy. Soc. **A254**, 163 (1960).
2. M. T. Laugier, Thin Solid Films **117**, 243 (1984).
3. P. J. Burnett and D. S. Rickerby, Thin Solid Films **157**, 233 (1988).
4. D. B. Marshall and A. G. Evans, J. Appl. Phys. **56** (10), 2632 (1984).
5. L. G. Rosenfeld, J. E. Ritter, T. J. Lardner and M. R. Lin, J. Appl. Phys. **67** (7), 3291 (1990).
6. M. P. de Boer and W. W. Gerberich, Acta Metall. Mater., in press (1996).
7. M. P. de Boer and W. W. Gerberich, Acta Metall. Mater., in press (1996).
8. J. A. Thornton, Ann. Rev. Mater. Sci. **7**, 239 (1977).
9. Z. Suo and J. W. Hutchinson, Int. J. Frac. **43**, 1 (1990).
10. A. M. Haghiri-Gosnet, F. R. Ladan, C. Mayeux, H. Launois and M. C. Joncour, J. Vac. Sci. Tech. **A7** (4), 2663 (1989).
11. T. W. Wu, J. Mater. Res. **6**, 407 (1991).
12. K. L. Johnson, *Contact Mechanics*, (Cambridge, Malta, 1985).
13. M. P. de Boer, J. C. Nelson and W. W. Gerberich, Proc. Roy. Soc. **A**, submitted (1996).
14. S. P. Timoshenko and J. N. Goodier, *Theory of Elasticity*, (Mc-Graw-Hill, New York, 1970).
15. M. P. de Boer and W. W. Gerberich, J. Mater. Res., submitted (1996).

### DISCLAIMER

This report was prepared as an account of work sponsored by an agency of the United States Government. Neither the United States Government nor any agency thereof, nor any of their employees, makes any warranty, express or implied, or assumes any legal liability or responsibility for the accuracy, completeness, or usefulness of any information, apparatus, product, or process disclosed, or represents that its use would not infringe privately owned rights. Reference herein to any specific commercial product, process, or service by trade name, trademark, manufacturer, or otherwise does not necessarily constitute or imply its endorsement, recommendation, or favoring by the United States Government or any agency thereof. The views and opinions of authors expressed herein do not necessarily state or reflect those of the United States Government or any agency thereof.